

Experimental Verification of Variable-Frequency Rocking Bearings for Near-fault Seismic Isolation

Lyan-Ywan Lu

*Department of Construction Engineering
National Kaohsiung First University of Science and Technology, Kaohsiung, Taiwan*

Tzu-Ying Lee

*Department of Civil Engineering,
National Central University, Taoyuan County, Taiwan.*

Chia-Chiea Hsu

National Kaohsiung First University of Science and Technology, Kaohsiung, Taiwan



SUMMARY

A near-fault earthquake usually possesses a long-period pulse-like component that may result in an excessive isolator displacement in a conventional isolation system, and consequently it will increase seismic risk or lead to an oversized isolator design. To alleviate this problem, a variable-frequency rocking-type bearing (VFRB) is proposed in this study. The proposed rocking bearing has a rocking surface with a variable curvature, and by properly selecting the geometry of the rocking surface, the isolation stiffness and frequency of the proposed rocking bearing become the functions of the bearing displacement. In order to experimentally verify its feasibility, a full-scale steel frame isolated by prototype VFRB bearings was tested by using a shaking table test in this study. The rocking surface of the prototype bearings were defined by a six-order polynomial function, so they have a relatively higher initial stiffness followed by a softening behavior. This mechanical property enable the VFRB isolation system to effectively suppress the excessive isolator displacement induced by a pulse-like near-fault earthquake, while retains a reasonable isolation efficiency. The test data show very good agreement with the simulated ones. Moreover, the experimental results demonstrate that the VFRB-isolated frame exhibits the desired behavior in a near-fault earthquake, and thus confirms the applicability of VFRB isolators for near-fault seismic isolation.

Keywords: rocking bearing, variable stiffness, variable frequency, near-fault isolation.

1. INTRODUCTION

Different from traditional seismic resistance techniques, the notion of seismic isolation is to implement a soft isolation layer under the protected structure, so the structure can be uncoupled from ground excitations (Naeim and Kelly 1999). A seismic structure with an isolation system is usually designed to be a long-period system with a fixed isolation frequency and damping ratio. This long-period feature inevitably induces a low-frequency resonant-like response when the isolation system is subjected to a ground motion containing strong long-period components. Many studies have confirmed that due to the long-period feature a base-isolated structure will incur excessive isolator displacement in near-fault earthquakes with a long-period pulse component (Jangid and Kelly 2001; Lu et al. 2002; Providakis 2008). Consequently, this will lead to an oversized isolator design or increase the risk of isolation pounding effect.

To avert this problem, some researchers have suggested using isolation systems with variable mechanical properties, so the isolation systems will not have resonant frequency and may be adaptive to a wider range of earthquakes with different characteristics (Nagarajaiah and Narasimhan 2006; Lu et al. 2011). As a part of research efforts for variable isolation systems, the objective of this study is to develop and test a new type of isolators called variable-frequency rocking bearings (VFRB), which have variable isolation stiffness and frequency that can meet the desired design specifications. In this paper, the theory and formulas that describe the mechanical properties of a general VFRB will be reviewed. Then, shaking table tests will be conducted to verify the developed VFRB theory, and the isolation performance of the prototype VFRB will be evaluated by using the test data. Additionally, in

the tests, particular attention will be paid to the seismic response of the VFRB system subjected to a near-fault earthquake.

2. MECHANICAL PROPERTIES OF A VARIABLE-FREQUENCY ROCKING BEARING (VFRB)

2.1. Restoring force of the VFRB

Fig. 1 shows the proposed rocking bearing installed under a structure footing. As shown in the figure, the rocking bearing has an articular (ball-and-socket) joint on the top and a rocking surface with a base plate on the lower part. The articular joint is connected to the super-structure through a mounting plate, while the base plate is mounted on the ground or the foundation of the structure. In an earthquake, the rocking surface of the bearing will rock back-and-forth on the base plate, thus the transmitted ground motion onto the super-structure can be mitigated. The rocking surface, which is usually axially symmetric, must be concaved and may have a variable curvature.

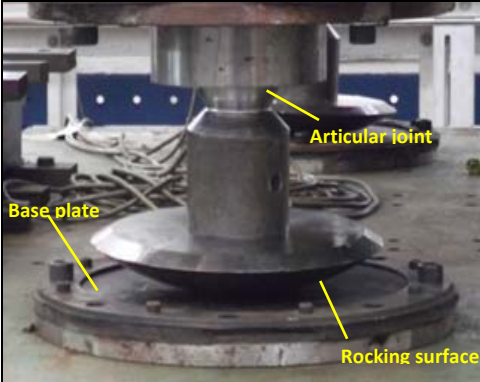


Figure 1. Photo of a prototype variable-frequency rocking bearing.

In this subsection, the formula describing the force-displacement relation of a general VFRB bearing will be given. Fig. 2 shows the free-body-diagram of the rocking bearing. In Fig. 2, there are two coordinate systems: x - y and X - Y coordinates. The x - y system is a fixed coordinates, while the X - Y system is a moving coordinates that is attached to the bearing and will rock along with the bearing. Also shown in Fig. 2, the rocking bearing has two major design parameters: the bearing height h and the geometric function $G(X)$ of the rocking surface. For the convenience, the function $G(X)$ is usually expressed in terms of the X - Y coordinates, i.e., $Y=G(X)$.

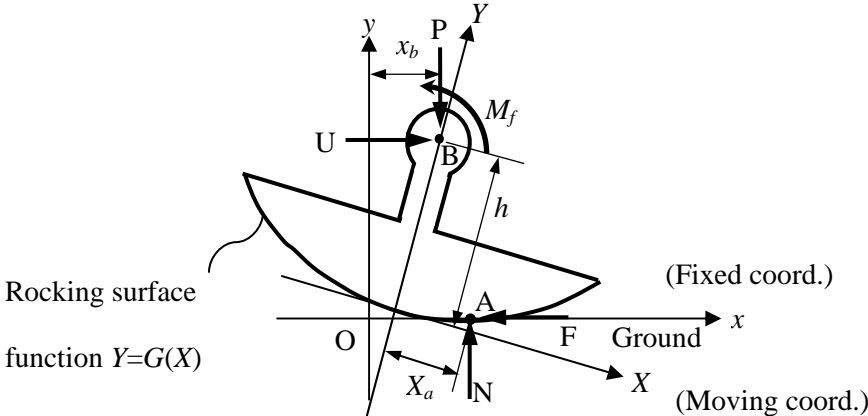


Figure 2. Free body diagram of the rocking bearing.

In Fig. 2, there are four forces and one moment applying on the bearing: P is the vertical load; N is the normal force applied on the contact point A of the rocking surface; F is the friction force applied on point A; U denotes the horizontal shear force that interacts between the bearing and the super-structure; M_f represents the moment caused by friction in the articular joint. Note that the shear U is equivalent to the horizontal seismic force transmitted to the super-structure. The shear U of the rocking bearing can be derived by taking the moment equilibrium equation about the contact point A. The derived total shear U can be written in the following form

$$U = u_r + u_f \quad (2.1)$$

The terms u_r and u_f in Eqn. 2.1 represent the restoring force and the friction force components in the total shear U , respectively. u_f is contributed by the friction moment M_f in the bearing, while u_r depends on the geometry of the bearing's rocking surface. The detail derivation of u_r and u_f were given in the reference (Lu et. al. 2009). While the derived u_f will be discussed later, the restoring force u_r can be written explicitly as

$$u_r = P\bar{u}_r, \text{ where } \bar{u}_r = \left[\frac{-(h - G(X_a))G'(X_a) + X_a}{h - G(X_a) + X_a G'(X_a)} \right] \quad (2.2)$$

In the above equations, X_a is the X-coordinate of the contact point A in X-Y coordinate system (see Fig. 2), and $G'(X)$ denotes the first derivative of $G(X)$ about variable X. Note that in Eqn. 2.2, $\bar{u}_r = u_r / P$ represents the normalized restoring force with respect to the bearing's vertical load P . Eqn. 2.2 demonstrates that the restoring force u_r of the rocking bearing is a function of X_a , $G(X)$ and h , and is proportional to the vertical load P . Note that as shown in Fig. 2, X_a is not the base displacement of the superstructure. The base displacement (or isolator displacement) should be defined as the horizontal displacement of point B denoted by x_b in Fig. 2. Point B is the center of the articular joint. Furthermore, because the horizontal displacement of point B is equal to the x-coordinate of point B in the x-y coordinate system, it can be derived that

$$x_b = \frac{(h - G(X_a))G'(X_a) - X_a}{\sqrt{1 + G'(X_a)^2}} + \int_0^{X_a} \sqrt{1 + G'(X)^2} dX \quad (2.3)$$

Investigating Eqns. 2.2 and 2.3, one should realize that it is difficult to directly express the restoring force u_r as an explicit function of the isolator displacement x_b . However, the relationship between u_r and x_b does exist and can be established through the intermediate variable X_a .

2.2. Restoring force of the rocking bearing

As mentioned previously, the friction moment M_f in the articular joint of the bearing causes the equivalent horizontal friction component u_f shown in Eqn. 2.1. At any time instant, the magnitude of u_f will rely on the current status of the bearing motion, which has two possible motion states, i.e., rocking and sticking (non-rocking) states. In the rocking state, the magnitude of u_f will be equal to its maximum value denoted by $u_{f,\max}$; while in the stick state, u_f depends on the present dynamic response of the isolated structure and its magnitude should not exceed $u_{f,\max}$. Therefore, u_f can be expressed as

$$\begin{aligned} |u_f| &< u_{f,\max} \quad (\text{for sticking state}) \\ |u_f| &< u_{f,\max} \quad (\text{for sticking state}) \end{aligned} \quad (2.4)$$

where

$$u_{f,\max} = \frac{r \sqrt{1 + G'(X_a)^2}}{h - G(X_a) + X_a G'(X_a)} \mu P \quad (2.5)$$

where μ and r represent the material friction coefficient and the radius of the articular joint, respectively. Eqn. 2.5 indicates that the maximum friction force $u_{f,\max}$ is also a function of X_a -coordinate. The complete derivation of Eqn. 2.5 is given in the article by Lu et. al. (2009).

2.3. Tangential isolation stiffness and isolation frequency

The tangential stiffness k_r (or called instantaneous stiffness) of the proposed bearing, which is defined as the rate of change of the restoring force, can be computed by taking the derivative of u_r with respect to the base displacement x_b , i.e.,

$$k_r(X_a) = \frac{du_r}{dx_b} = \frac{du_r(X_a)/dX_a}{dx_b(X_a)/dX_a} = \frac{P \bar{u}'_r(X_a)}{x'_b(X_a)} \quad (2.6)$$

In the last equation, u_r defined in Eqn. 2.2 has been applied. Eqn. 2.6 implies that the isolation stiffness is not a constant but a function of the base displacement x_b , since $X_a = X_a(x_b)$. Furthermore, by using Eqn. 2.6, the tangential isolation frequency ω_b can be computed by the following equation

$$\omega_b(X_a) = \sqrt{\frac{k_r(X_a)}{M}} = \sqrt{\frac{P \bar{u}'_r(X_a)}{M x'_b(X_a)}} = \sqrt{\frac{g \bar{u}'_r(X_a)}{x'_b(X_a)}} \quad (2.7)$$

where M is the mass of the super-structure. Notably, in Eqn. 2.7 it is assumed that the superstructure behaves like a rigid body, and the vertical load P due to the structural weight can be expressed as $P = M g$. From Eqn. 2.7, it is evident that isolation frequency of the bearing is not a constant, but is an implicit function of the base displacement x_b and the geometric function $G(X)$, since \bar{u}'_r is a function of $G(X)$ (see Eqn. 2.2). It is for this reason that the proposed bearing is called the variable-frequency rocking bearing. Eqn. 2.7 also demonstrates that the isolation frequency of the PRB is completely independent from the structural mass M . By properly selecting the geometric function $G(X)$ of the rocking surface, the isolated system may possess favourable dynamic characteristics in different base displacement.

3. DEFINING THE ROCKING SURFACE BY A POLYNOMIAL FUNCTION

In the shaking table tests of this study, the geometric function $G(X)$ of the prototype VFRB bearings is defined by the following sixth-order polynomial function

$$G(X) = c_1 X^6 + c_2 X^4 + c_3 X^2 \quad (3.1)$$

where c_1 , c_2 and c_3 are the three constant coefficients. The above polynomial function is an even function, which is symmetric about the Y -axis and passes through the origin of the X - Y coordinates. Since the shape of such a bearing is defined by a polynomial, the bearing is called a *Polynomial Rocking Bearing* (PRB) hereafter. Furthermore, after $G(X)$ is substituted from Eqn. 2.8 in Eqns. 2.2 and 2.5, both the restoring force u_r and maximum friction force $u_{f,\max}$ of the PRB become functions of three polynomial coefficients, c_1 , c_2 and c_3 . The selection of these three coefficients is an important task in designing the PRB, since they determine the mechanical properties of the PRB.

Lu et al. (2011) studied sliding isolators with variable curvature (SIVC) whose stiffness is also a function of the isolator displacement. Their results indicate that an SIVC with a relatively higher initial

stiffness followed by softening mechanical behavior (decreasing stiffness) is preferable for near-fault seismic isolation, because it is able to effectively suppress the excessive isolator displacement induced by a severe long-period earthquake without significantly increasing the superstructure acceleration. To define the restoring force u_r as a function of the isolator displacement x_b , they also suggested a fifth-order polynomial function with specific coefficient values for u_r . Based on the function u_r suggested by Lu *et al.* (2011), the values of the coefficients c_1 , c_2 and c_3 for the PRB used in the present study are chosen as listed in Table 1. As a result, Fig. 3 shows the normalized restoring force (u_r/P) and the isolation period $T (= 2\pi/\omega_b)$ as functions of the bearing displacement x_b . Fig. 3(a) shows that the PRB has a relatively higher initial stiffness at $x_b = 0$, but the stiffness swiftly decreases as x_b increases, until x_b reaches the critical displacement of 0.08m, beyond which the bearing stiffness increases along with x_b . Moreover, Fig. 3(b) shows that the PRB has an initial isolation period of about 1 second at $x_b = 0$, which is shorter than the commonly used isolation periods, but the isolation period T is swiftly prolonged to more than 7 seconds at $x_b = 0.08$ m, beyond which T is shortened due to the increased isolation stiffness.

Table 1. Parameters of prototype PRB isolators used in the test.

Geometric Parameter		Value	Material parameter	Property
Polynomial coefficient of rocking surface	c_1	-603.5 (1/m ⁵)	Ball socket	Brass
	c_2	45.14 (1/m ³)	Spherical head	Steel
	c_3	1.307 (1/m)	Rocking surface	Steel
Bearing height h		0.187 m	Base plate	Rubber
Radius of ball head r		0.044 m	Material friction coeff. μ	0.30

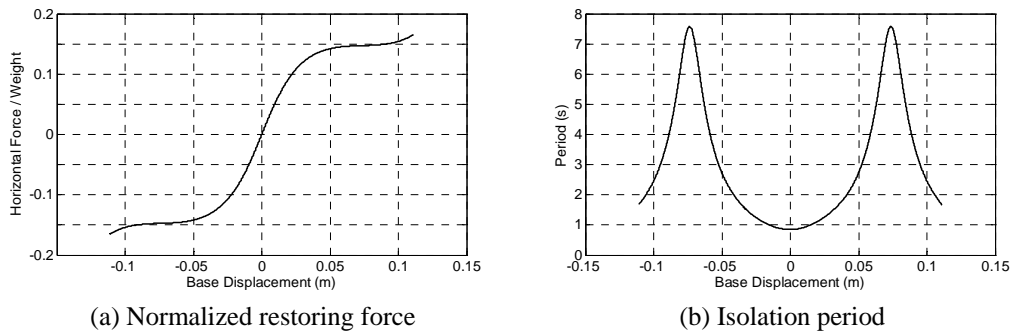


Figure 3. Mechanical properties of the prototype PRB bearings.

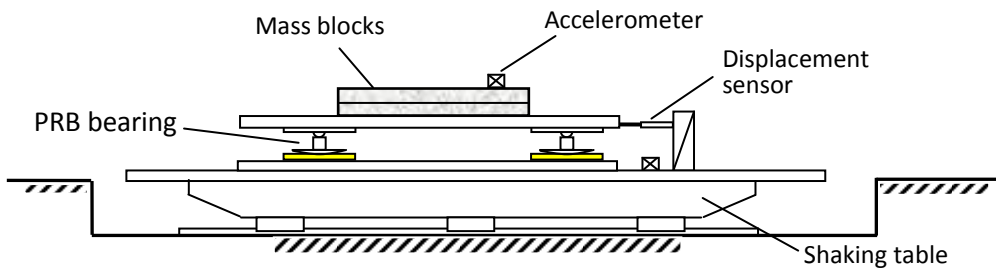


Figure 4. Mechanical properties of the prototype PRB bearings.

4. HYSTERETIC PROPERTY TEST OF THE PROTOTYPE PRB SYSTEM

In order to verify experimentally the general theory of the VFRB discussed in the previous sections, two types of shaking table tests were conducted: (1) a hysteretic property test of the PRB system, and (2) a seismic test of a PRB isolated structure. Table 1 lists all the constituent materials and parametric values for the prototype PRB bearings used in the tests. Figure 4 depicts the setup of the first test, which involved four PRB bearings mounted under the four corners of a rigid object of a total weight

about $W=10.4\text{kN}$. Because the purpose of this test is simply to observe whether the hysteretic property of the tested PRB system follows the derived formulas, the dynamic effect of the superstructure was eliminated by using the rigid mass blocks as the isolated object. In the test, a sinusoidal horizontal excitation of frequency 1 Hz and amplitude 0.14g was imposed on the tested PRB system. The acceleration and displacement of the isolation system were all recorded by an accelerometer and displacement sensor, as shown in Fig. 4.

Based on the measured data, Fig. 5 compares the experimental and theoretical hysteresis loops of the overall PRB isolation system. The total shear forces of both loops have been normalized with respect to the vertical load. Notably, the experimental shear force in Fig. 5(a) is obtained indirectly by multiplying the acceleration of the isolated object with its mass. On the other hand, the theoretical force plotted in Fig. 5(b) is simulated by using Eqns. 2.1, 2.2 and 2.4 with the parameters listed in Table 1. Figure 5 shows that the experimental hysteresis loop matches the theoretical one very well, and the prototype PRB system has the desired mechanical properties. It also indicates that the formulas derived in Section 2 are able to simulate the hysteretic behavior of a VFRB isolation system. In the next section, these formulas will be applied to simulate the seismic responses of a steel structure isolated by the prototype PRB system, so their application to a more realistic case can be further verified.

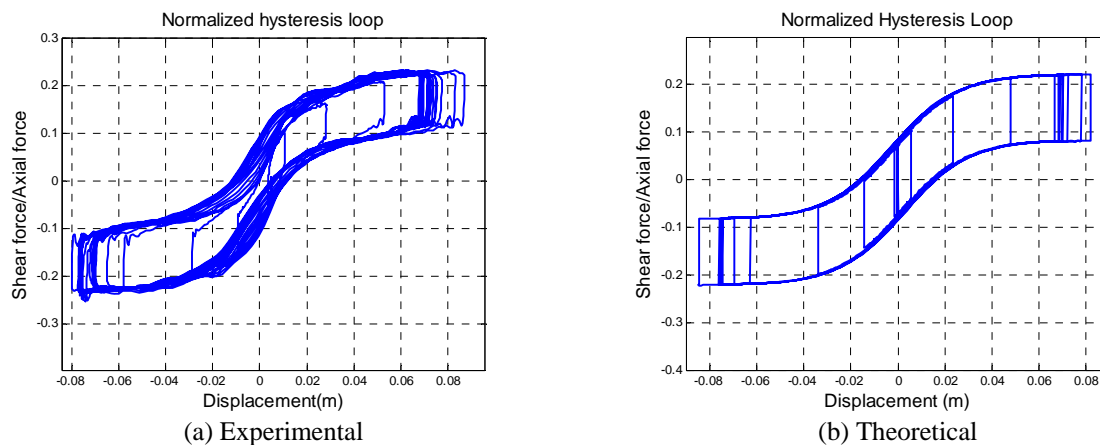


Figure 5. Comparison of normalized hysteresis loops for the prototype PRB system.

5. SEISMIC TEST OF A PRB-ISOLATED STRUCTURE

5.1. Test setup

Figure 6 shows the setup of the second shaking table test that involves a full-scale one-story steel frame isolated by the prototype PRB bearings mounted under each column of the frame. While the properties of the bearings have been listed in Table 1, Table 2 summarizes the structural parameters of the steel frame. The steel frame is 3m high and has the plane dimension of 3m x 2m (length by width). The total mass of the frame is about 12.8 metric tons. The results of a system identification test show that the steel frame has a fundamental frequency (fixed base) of about 2.17 Hz and a damping ratio of 2.1%.

To investigate the isolation performance of the PRB-isolated frame in different earthquakes, two types of historic ground motions with very different characteristics were considered as the excitations in the test. Imposed on the isolated frame along its longer 3m side, the two ground motions are: (1) the El Centro earthquake of 1940, which is used to represent a ground excitation that is widely used in earthquake engineering research to represents typical far-field earthquake in this study. (2) The Imperial Valley earthquake (El Centro Array 6), which was recorded by a station near a tectonic fault in 1979, and is used to represent a near-fault earthquake in this study.

Table 2. Structural parameters of the steel frame used in the test.

Property	Value	Property	Value
Material	H-shaped steel	Natural frequency ω_s	2.17 Hz
Structural dimension	3 m \times 3m \times 2m	Damping ratio ζ_s	2.1 %
Top-floor mass m_s	5.91 tons	Structural stiffness k_s	1099 kN/m
Base-floor mass m_b	6.91 tons	Damping coefficient c_s	3.38 kN-s/m

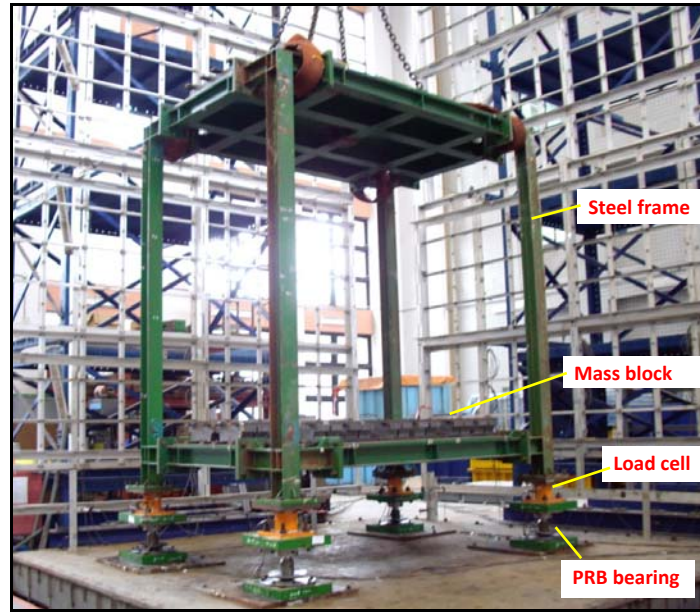


Figure 6. Test setup of the PRB-isolated steel frame.

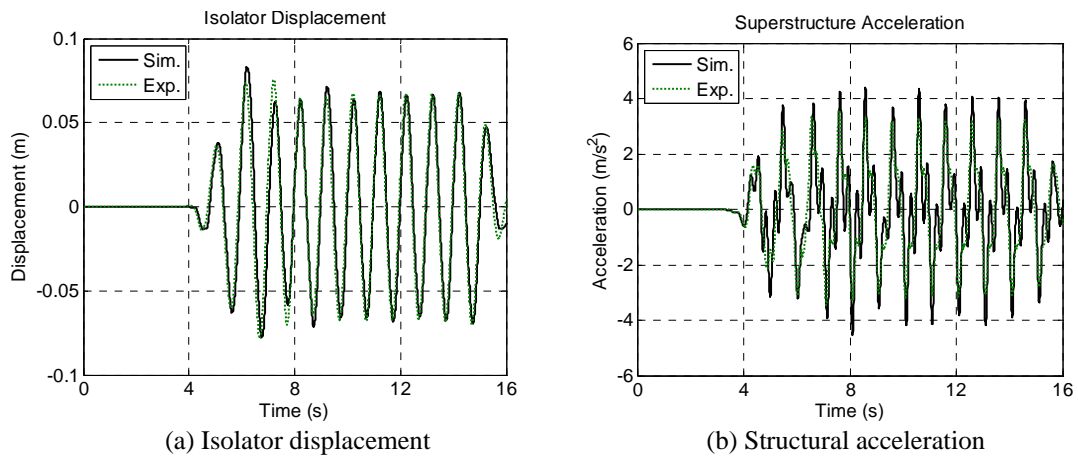


Figure 7. Comparison of experimental and theoretical responses of the PRB isolated frame under a harmonic excitation (frequency=1Hz; amplitude=1.7m/s²).

5.2. Comparison of experimental and theoretical responses

To verify the PRB theory discussed previously, Fig. 7 compares the experimental and simulated responses of the PRB-isolated frame under harmonic excitation, which has a frequency of 1 Hz and amplitude of 1.7 m/s². In the simulated results of Fig. 7, the parametric values given in Tables 1 and 2

are used for the PRB and structural systems, respectively. Additionally, the axial load P of the PRB system is taken to be the total weight of the isolated frame and remains constant. Figs. 7(a) and 7(b) show that the simulated isolator displacement and structural acceleration match very well with the measured ones. This indicates that the theory and numerical method discussed in the previous sections are applicable for the analysis of the dynamic response of a PRB-isolated structural system. Additionally, it also confirms that the test data measured by the sensors are reliable.

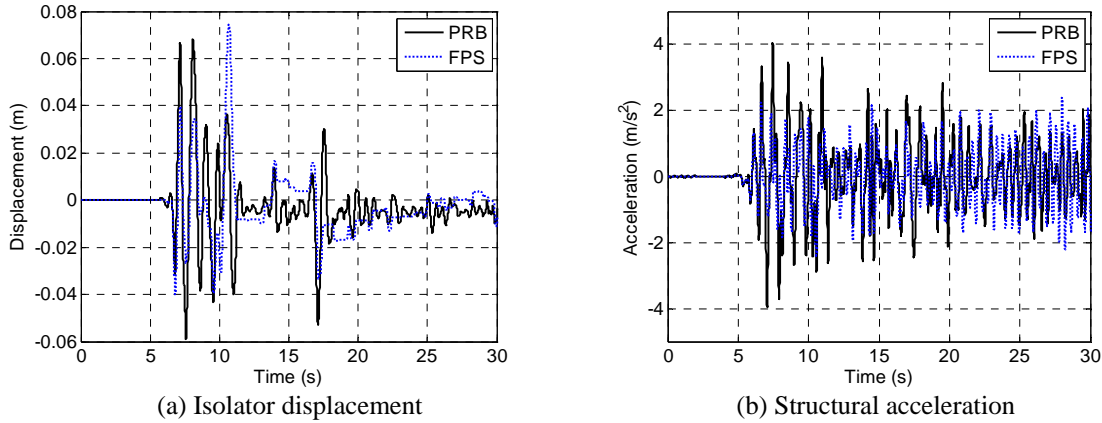


Figure 8. Comparison of the PRB and FPS responses under the far-field earthquake (El Centro; $PGA=4.6m/s^2$).

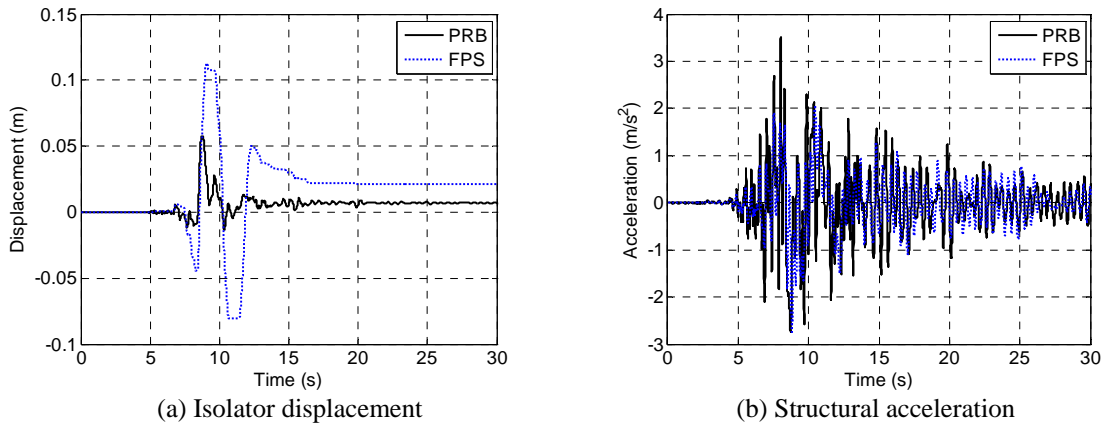


Figure 9. Comparison of the PRB and FPS responses under the near-fault earthquake (Imperial Valley; $PGA=4.1m/s^2$).

5.3. Comparison of isolation responses of PRB and FPS

To evaluate the isolation efficiency of the PRB, in this subsection, the measured time-history responses of the PRB-isolated frame is compared to the simulated responses of the same frame isolated by conventional friction isolators, in this case FPS isolators. For a fair comparison, the simulated FPS-isolated frame will share the same structural parameters listed in Table 2, and also use the same ground excitations measured from the shaking table test. Furthermore, in the simulation, a typical isolation period of t_{iso} seconds was adopted for the FPS system, while the friction coefficient of the FPS is taken to be $\mu_{FPS} = 0.07$, which is the same as the initial equivalent friction coefficient of the PRB (see Fig. 5). Figure 8 compares the time-history responses of the steel frame with the PRB and FPS systems when both systems are subject to the El Centro earthquake (the far-field earthquake) with $PGA=4.6m/s^2$, while Fig. 9 compares the responses for the Imperial Valley earthquake (the near-fault earthquake) with $PGA=4.1m/s^2$. Figure 8 shows that in the far-field earthquake the PRB and FPS have roughly equal peak isolator displacements, but the PRB induces slightly higher superstructure acceleration. On the other hand, in the near-fault earthquake, Figure 9 demonstrates that

the PRB effectively suppresses about 55% of the isolator displacement of the FPS, without significantly amplifying the acceleration response of the superstructure.

6. CONCLUSIONS

In order to alleviate the problem of excessive isolator displacement encountered in near-fault earthquakes, a variable isolation system composed of variable-frequency rocking bearings (VFRB) was experimentally studied in this work. By properly selecting the geometry of the rocking surface of the bearings, the isolation frequency of the VFRB bearings becomes a function of the bearing displacement, and is exclusively determined by the bearing geometric parameters and independent of the structural mass. To improve the isolation performance under near-fault earthquakes, this study proposed a sixth-order polynomial function to define the rocking surface of the prototype bearings used in the test. Two types of shaking table tests were conducted for the prototype VFRB system. The conclusions of the tests are summarized below.

(1) In the first shaking table test, a rigid mass block isolated by the prototype bearings was tested, in order to obtain the hysteretic diagram of the VFRB system itself without the dynamic effect of the superstructure. The test results show that the experimental hysteresis loop matches fairly well with the theoretical one. This confirms that the derived VFRB theory is able to capture the variable hysteretic property of the bearing, and the VFRB is a feasible way to achieve the techniques of passive variable isolation.

(2) By properly selecting the coefficient values of the six-order polynomial function that defines the bearing rocking surface, the prototype bearings have a relatively higher initial stiffness followed by a softening behavior. Because of this mechanical feature, the test results show that as compared to the response of a FPS system, the VFRB isolation system is able to effectively suppress the large isolator displacement induced by a strong near-fault earthquake ($PGA=4.1$), while retaining equal reduction rate on the super-structural acceleration. This indicates that the VFRB can be a promising technology for near-fault seismic isolation.

ACKNOWLEDGEMENT

This research was financially supported by the National Science Council of R.O.C. (Taiwan) through Grant NSC100-2625-M-327-001, and technically supported by the National Center for Research on Earthquake Engineering (NCREE, Taipei). The first author is also grateful to his former graduate students Mr. I-Ling Yeh and Mr. Shih-Wei Yeh for processing the test data.

REFERENCES

- Jangid, R.S. and Kelly, J.M. (2001). Base isolation for near-fault motions. *Earthquake Engineering and Structural Dynamics*. **30**:5,691-707.
- Lu, L.Y., Shih, M.H., Chang Chien, C.S. and Chang, W.N. (2002). Seismic performance of sliding isolated structures in near-fault areas. *Proceedings of the 7th US National Conference on Earthquake Engineering, July 21-25, Boston, MA, USA*. Session AT-2.
- Lu, L.Y., Lee, T.Z., Yeh, I.L. and Chang, H. (2009). Rocking Bearings with Variable Frequency for Near-fault Seismic Isolation (in Chinese). *Journal of the Chinese Institute of Civil and Hydraulic Engineering*. under review, submitted in February.
- Lu, L.Y., Lee, T.Y. and Yeh, S.W. (2011). Theory and experimental study for sliding isolators with variable curvature. *Earthquake Engineering and Structural Dynamics*. **40**:14,1609-1627.
- Providakis, C.P. (2008). Effect of LRB isolators and supplemental viscous dampers on seismic isolated buildings under near-fault excitations. *Engineering Structures*. **30**:5,1187-1198.
- Nagarajaiah, S. and Narasimhan, S. (2006). Smart base isolated benchmark building Part II: Phase I Sample controllers for linear isolation system. *Journal of Structural Control and Health Monitoring*. **13**:2-3,589-604.
- Naeim, F. and Kelly, J.M. (1999). Design of Seismic Isolated Structures: from theory to practice, John Wiley & Sons.